Substrate and product specificities of *cis*-type undecaprenyl pyrophosphate synthase

Annie P.-C. CHEN*, Sing-Yang CHANG†, Yu-Chung LIN‡, Yang-Sheng SUN†, Chao-Tsen CHEN‡, Andrew H.-J. WANG*† and Po-Huang LIANG*†[1]

*Institute of Biochemical Sciences, National Taiwan University, Taipei 106, Taiwan, Republic of China, †Institute of Biological Chemistry, Academia Sinica, 128 Academia Road, Taipei 115, Taiwan, Republic of China, and ‡Department of Chemistry, National Taiwan University, Taipei 106, Taiwan, Republic of China

UPPS (undecaprenyl pyrophosphate synthase) catalyses consecutive condensation reactions of FPP (farnesyl pyrophosphate) with eight isopentenyl pyrophosphates to generate C_{55} UPP, which serves as a lipid carrier for bacterial peptidoglycan biosynthesis. We reported the co-crystal structure of *Escherichia coli* UPPS in complex with FPP. Its phosphate head-group is bound to positively charged arginine residues and the hydrocarbon moiety interacts with hydrophobic amino acids including L85, L88 and F89, located on the $\alpha 3$ helix of UPPS. We now show that the monophosphate analogue of FPP binds UPPS with an eight times lower affinity ($K_d = 4.4\ \mu$M) compared with the pyrophosphate analogue, a result of a larger dissociation rate constant ($k_{off} = 192\ \text{s}^{-1}$). Farnesol (1 mM) lacking the pyrophosphate does not inhibit the UPPS reaction. GGPP (geranylgeranyl pyrophosphate) containing a larger C_{20} hydrocarbon tail is an equally good substrate ($K_m = 0.3\ \mu$M and $k_{cat} = 2.1\ \text{s}^{-1}$) compared with FPP. The shorter C_{10} GPP (geranyl pyrophosphate) displays a 90-fold larger K_m value ($36.0 \pm 0.1\ \mu$M) but similar k_{cat} value ($1.7 \pm 0.1\ \text{s}^{-1}$) compared with FPP. Replacement of L85, L88 or F89 with Ala increases FPP and GGPP K_m values by the same amount, indicating that these amino acids are important for substrate binding, but do not determine substrate specificity. With GGPP as a substrate, UPPS still catalyses eight isopentenyl pyrophosphate condensation reactions to synthesize C_{60} product. Computer modelling suggests that the upper portion of the active-site tunnel, where *cis* double bonds of the product reside, may be critical for determining the final product chain length.

Key words: computer modelling, prenyltransferase, product specificity, site-directed mutagenesis, substrate specificity, undecaprenyl pyrophosphate synthase.

INTRODUCTION

A group of prenyltransferases catalyse chain elongation of C_{15} FPP (farnesyl pyrophosphate) (allylic substrate) to designated chain lengths through condensation reactions with specified numbers of C_5 IPP (isopentenyl pyrophosphate) (homoallylic substrate) [1–3]. According to the stereochemistry of the double bonds formed from each IPP condensation, these prenyltransferases are classified as *cis*- or *trans*-type [4]. The *trans*-type prenyltransferases, such as OPPS (octaprenyl pyrophosphate synthase), bind FPP and IPP substrates presumably through two conserved Asp-rich DDXXD motifs, which chelate the Mg^{2+} ion to bind the pyrophosphate group [5–7]. In contrast, the *cis*-type UPPS (undecaprenyl pyrophosphate synthase) that catalyses consecutive condensation reactions of FPP with eight molecules of IPP to form the C_{55} product, binds its substrates through H-bonds, and through charged and hydrophobic interactions [8–10]. The enzyme product serves as a lipid carrier to transport lipid II (made in the cytoplasm) across the cell membrane for bacterial peptidoglycan biosynthesis [11]. UPPS is the first and the only *cis*-prenyltransferase whose three-dimensional structure has been solved and is being intensively studied as a model to understand the catalytic mechanism of *cis*-prenyltransferases [12]. Moreover, UPPS may serve as a new antibiotic target since it has been proven to be essential for bacterial survival [13].

We have solved the crystal structures of UPPS alone, the enzyme in complex with substrate and product analogues (ammonium sulphate and Triton X-100), and also the complex with the FPP substrate [9,10,12]. In this structure, FPP is bound at the top of the tunnel-shaped active site surrounded by the two α-helices ($\alpha 2$ and $\alpha 3$) and four β-strands (βA, βB, βD and βC) as shown in Figure 1(A) [9]. On the basis of the crystal structure [10], the pyrophosphate group of FPP is bound to the backbone NHs of G29 and R30 as well as to the side chains of N28, R30 and R39 through hydrogen bonds (Figure 1B). It was not determined how the pyrophosphate head group and the hydrocarbon tail of FPP contribute to the enzyme–substrate interaction. Previously, we synthesized an FPP analogue TFMC-GPP [7-(2,6-dimethyl-8-pyrophospho-2,6-octadienyloxy)-8-methyl-4-trifluoromethyl-chromen-2-one], incorporating a fluorescent trifluoromethyl-chromen-2-one cross-linking to C_{10}-GPP (geranyl pyrophosphate) [14]. In the present study, we have synthesized TFMC-GP [7-(2,6-dimethyl-8-phospho-2,6-octadienyloxy)-8-methyl-4-trifluoromethyl-chromen-2-one], containing a monophosphate group as a probe to evaluate its enzyme binding affinity, in comparison with the diphosphate substrate analogue and the phosphate-free farnesol.

For testing the enzyme–substrate interaction mediated by the hydrocarbon moiety of the allylic substrate, reaction kinetics parameters for using all-*trans* C_{10}-GPP and C_{20}-GGPP (genanyl-geranyl pyrophosphate) as alternative allylic substrates were determined. The possibility of using FPP or GPP as a homoallylic substrate was also tested. The hydrocarbon moiety of FPP is bound to the hydrophobic amino acids including L85, L88 and F89,
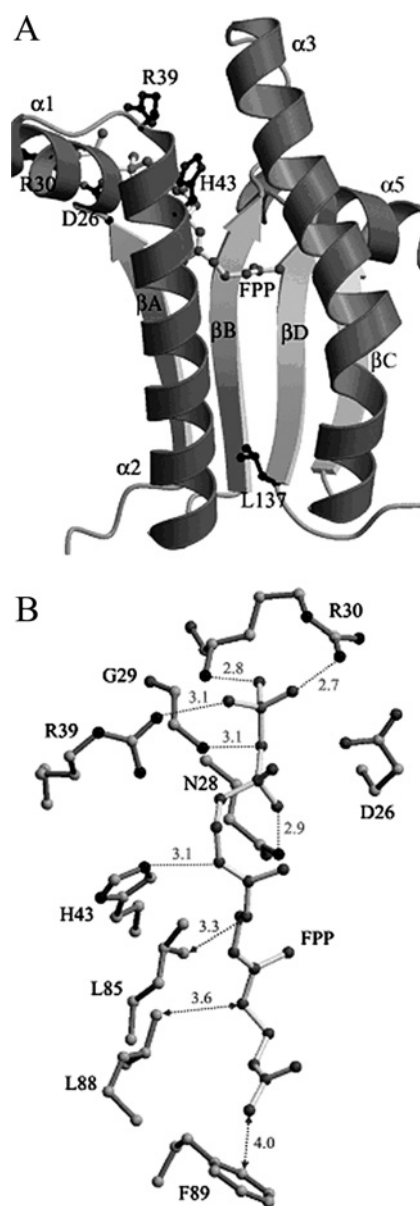
Figure 1   Three-dimensional structure of UPPS in complex with FPP

(**A**) The active site portion of UPPS surrounded by two α-helices (α2 and α3) and four β-strands (βA, βB, βD and βC) and bound FPP on the top of the tunnel is shown based on our published structure [10]. At the bottom of the tunnel, the large amino acid L137 acts as a seal to block further chain elongation and determine the chain length of the product [12]. The catalytically important amino acids including D26, H43, R30 and R39 near FPP are displayed. (**B**) The pyrophosphate of FPP is hydrogen-bonded to the backbone NH and side chain of R30, and backbone NH of G29 as well as the side-chains of R39 and N28 [10]. The hydrocarbon moiety of FPP is bound with hydrophobic amino acids including L85, L88 and F89, located on the α3 helix that moves towards the substrate during FPP binding. The distances are shown in Å (1 Å = 0.1 nm).

located on the α3 helix. These amino acids were mutated to probe the roles of L85, L88 and F89 in substrate recognition.

FPP is elongated by condensation with eight IPP molecules towards the bottom of the tunnel sealed by the large amino acid L137 (see Figure 1A), which blocks further chain elongation and determines the final chain length of the C_{55}-product [12]. The reason why *cis*-prenyltransferases synthesize longer chain-length products than the *trans*-prenyltransferases has long been puzzling. As shown in the present study, the structure of C_{60}-products
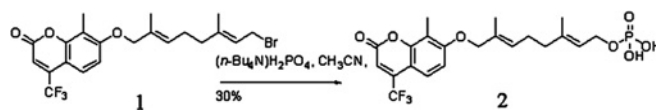
Scheme 1   Synthesis of compound 2 from previously prepared compound 1 [14]

resulting from the larger C_{20}-GGPP substrates predicted by computer modelling is compared with that of the assumed C_{60}-product synthesized from FPP and one extra IPP. On the basis of the results, we propose that the molecular shapes of both the active site of UPPS and its product are essential to determine the ultimate product chain length.

EXPERIMENTAL

Materials

Radiolabelled [^{14}C]IPP (55 mCi/mmol) was purchased from Amersham Biosciences and FPP was obtained from Sigma. *Taq* DNA polymerase was obtained from Life Technologies. The plasmid mini-prep kit, the DNA gel extraction kit and the Ni^{2+}-nitrilotriacetate resin were purchased from Qiagen. Potato acid phosphatase (2 units/mg) was purchased from Roche Molecular Biochemicals. FXa and the protein expression kit (including the pET32Xa/LIC vector and competent JM109 and BL21 cells) were obtained from Novagen. All commercial buffers and reagents were of the highest grade available.

Synthesis of TFMC-GP

The synthetic route for compound 2 (TFMC-GP) is shown in Scheme 1. To the solution containing 7-(8-bromo-2,6-dimethyl-2,6-octadienyloxy)-8-methyl-1,4-trifluoromethyl-chromen-2-one (compound 1) (230 mg, 0.5 mmol), which was synthesized according to our reported procedure [14], and CH_3CN (2 ml), was added tetrabutylammonium dihydrogen phosphate (340 mg, 1.0 mmol) in 6 ml of CH_3CN at 25 °C. The solution was stirred at room temperature (25 °C) for 6 h. After evaporation of solvent, the residue was dissolved in 3 ml of propan-2-ol/water (1:1) mixture and loaded on to an anion-exchange column of Dowex AG50X80 (NH$_4^+$ form) eluted with propan-2-ol/water (1:1) to give the crude product. The desired fractions were collected, the organic solvent was removed by a rotary evaporator and the remaining water was freeze-dried to yield a white solid. The solid was further purified by reversed-phase HPLC using a program of 20 % B (80 % A) for 5 min, followed by a linear gradient of 20 % B (80 % A) to 100 % B (0 % A) over 30 min with a flow rate of 2.5 ml/min [where A = 25 mM aqueous ammonium bicarbonate (pH 8.0), B = acetonitrile]. The desired peak was collected, frozen and freeze-dried to afford the final product TFMC-GP (30 %). ^{1}H NMR (400 MHz, CD$_3$OD) δ 1.68 (s, 3H), 1.73 (s, 3H), 2.07 (t, 2H, $J = 7.6$ Hz), 2.21 (m, 2H), 2.27 (s, 3H), 4.39 (t, 2H, $J = 6.8$ Hz), 4.57 (s, 2H), 5.39 (t, 1H, $J = 6.8$ Hz), 5.58 (t, 1H, $J = 6.8$ Hz), 6.69 (s, 1H), 7.07 (d, 1H, $J = 9.2$ Hz), 7.58 (d, 1H, $J = 9.2$ Hz); ^{13}C NMR (100 MHz, CD$_3$OD) δ 7.55, 13.10, 15.64, 25.99, 38.91, 62.05, 74.66, 107.05, 109.76, 111.69 (q, $J = 6.1$ Hz), 114.73, 121.52 (q, $J = 8.3$ Hz), 121.98 (q, $J = 273.1$ Hz), 123.55, 128.81, 130.70, 139.39, 142.08 (q, $J = 31.9$ Hz), 153.22, 160.74, 160.98; ^{31}P NMR (162 MHz, CD$_3$OD) δ 6.30; UV (H$_2$O), λ$_{max}$ = 336 nm, ε = 10 700 M^{-1}·cm^{-1}; IR: (KBr) 3449, 1738, 1610, 1101; FAB-MS: *m/z* 477.1 (M + H$^+$), HRMS (FAB): *m/z* calculated for $C_{21}H_{25}F_3O_7P$ (M + H$^+$): 477.1290, found: 477.1288.

Measurement of the inhibition constant for TFMC-GP

Measurement of the inhibition constant for TFMC-GP was performed in a reaction mixture containing 0.03 μM UPPS, 3 μM FPP and 50 μM [^{14}C]IPP in a buffer of 100 mM Hepes/KOH (pH 7.5), 50 mM KCl, 0.5 mM MgCl$_2$ and 0.1 % Triton X-100 in the presence of various concentrations of the inhibitor. Triton X-100 (0.1 %) was included in the reaction mixture so that product release did not limit the reaction, thus allowing the measurement of the IPP condensation rate at each inhibitor concentration [15]. Portions of the reaction mixture were periodically withdrawn and mixed with 10 mM EDTA to terminate the reaction and 1-butanol was utilized to extract the radiolabelled products for quantification using scintillation counting. The initial rates were obtained in the presence of 0–50 μM inhibitor and IC$_{50}$ and K_i values of the inhibitor were determined by fitting the plot of reaction rates versus the inhibitor concentrations using the following equations [16]

$$A(I) = A(0)\{1 - [I/(I + K_i(1 + S/K_m))]\} \tag{1}$$

$$IC_{50} = K_i(1 + S/K_m) \tag{2}$$

In these equations, $A(I)$ is the enzyme activity with the inhibitor concentration I, $A(0)$ enzyme activity without inhibitor, I the inhibitor concentration, K_i the inhibition constant of the inhibitor, S the FPP concentration and K_m the Michaelis constant for FPP.

Fluorescence titration experiments

The fluorescence spectrum of 1 μM TFMC-GP was collected before and after the addition of 1 μM UPPS in a buffer containing 100 mM Hepes/KOH (pH 7.5), 50 mM KCl and 0.5 mM MgCl$_2$ at 25 °C. The spectra were also collected after the addition of 1, 2 and 3 μM FPP to outcompete TFMC-GP.

Measurements of k_{on} and k_{off} of the TFMC-GP using stopped-flow technology

The binding constant k_{on} and release constant k_{off} of the monophosphate FPP analogue (TFMC-GP) were measured using stopped-flow methods as described previously [14]. The compound's fluorescence above 530 nm (using a cut-off filter) was monitored using an excitation wavelength of 336 nm. In the measurements of k_{on}, each concentration of UPPS (2.5, 3.75, 5 or 6.5 μM) was mixed with an equal volume of 0.5 μM TFMC-GP solution in a buffer containing 100 mM Hepes/KOH (pH 7.5), 0.5 mM MgCl$_2$ and 50 mM KCl. The stopped-flow trace (average of four runs) monitored with time was fitted with the exponential equation shown below (eqn 3) (which was provided with the machine) to give the observed rate constant k_{obs} for each enzyme concentration. The concentrations cited in parentheses and hereafter in the text are those after mixing. The slope of k_{obs} versus enzyme concentration yielded the rate constant k_{on} for the compound binding to UPPS. In the measurement of the dissociation rate constant k_{off}, UPPS (0.5 μM) preincubated with TFMC-GP (7.5 μM) was mixed with an excess of competitor, FPP (25 μM). The stopped-flow trace was fitted with a single exponential equation (eqn 3) to obtain the k_{off} for the compound. The K_d value for the compound binding to the UPPS was obtained from k_{off}/k_{on}.

$$F_t = F_c - (F_o - F_c)\exp(-k_{obs}t) \tag{3}$$

In the above equation, F_t is the fluorescence at a given time point t, F_c the end-point fluorescence, F_o the initial fluorescence and k_{obs} the observed rate constant.

Site-directed mutagenesis of UPPS

UPPS mutants were prepared by using PCR techniques in conjunction with the *Escherichia coli Bos-12* UPPS gene template in the pET32Xa/Lic vector as described previously [17]. The mutagenic primers used were prepared by MDBio (Taipei, Taiwan). The mutagenic oligonucleotides for performing site-directed mutagenesis are as follows: 5′-AGTGCGGCAATGGA-ACTG-3′ for L85A (Leu^{85} → Ala), 5′-ATGGAAGCGTTTGTG-TGG-3′ for L88A and 5′-GAACTGGCTGTGTGGGCG-3′ for F89A. Subsequently, the forward primer 5′-GGTATTGAGGGT-CGCATGTTGTCTGCT-3′ and reverse primer 5′-AGAGGAGA-GTTAGAGCCATCAGGCTGT-3′ were used in combination with the PCR products obtained using the above mutagenic oligo-nucleotides to create the full-length mutant UPPS genes. The FXa cleavage site (IEGR) and the complementary sequences to the sticky ends of the linear vector pET-32Xa/LIC were included in these primers. Using a thermocycler (Applied Biosystems), 30 cycles of PCR were performed with the melting temperature at 95 °C for 2 min, annealing temperature at 42 °C for 1 min and polymerization temperature at 68 °C for 1 min. The PCR product was subjected to electrophoresis on 1.2 % agarose gel in TAE buffer (40 mM Tris-acetate, pH 8, 1 mM EDTA), and the gel was then stained with ethidium bromide. The part of the gel containing the band of the correct size was excised, and the DNA was re-covered using a DNA elution kit. The constructed gene of a mutant enzyme was ligated to the pET32Xa/LIC vector by incubation for 1 h at 22 °C. The recombinant UPPS plasmid was then used to transform *E. coli* JM109 competent cells that were streaked on an LB (Luria–Bertani) agar plate containing 100 μg/ml ampicillin. Ampicillin-resistant colonies were selected from the agar plate and grown in 5 ml of LB culture containing 100 μg/ml ampicillin overnight at 37 °C. The mutation was confirmed by sequencing the entire UPPS mutant gene of the plasmid obtained from the overnight culture. The correct construct was subsequently trans-formed to *E. coli* BL21 for protein expression. A 5 ml overnight culture of a single transformant was used to inoculate 500 ml of fresh LB medium containing 100 μg/ml ampicillin. The cells were grown to $A_{600} = 0.6$ and induced with 1 mM isopropyl β-D-thiogalactoside. After 4–5 h, the cells were harvested by centri-fugation at 7000 *g* for 15 min. The purification of mutant UPPS was according to our reported procedure using Ni^{2+}-nitrilo-triacetate column chromatography and FXa for tag removal [17].

Measurements of K_m and k_{cat} values for wild-type and mutant UPPS

For the measurements of kinetic parameters, wild-type or mutant UPPS (0.01 μM wild-type, 0.3 μM L85A, 0.1 μM L88A or 0.1 μM F89A) was added to initiate the reaction of FPP or GGPP with [^{14}C]IPP in 200 μl solutions. For K_m and k_{cat} determinations, a large range of substrate concentrations was used to estimate the K_m for each substrate first. To measure accurately the IPP K_m value, 5 μM FPP was utilized to saturate the enzyme, and IPP con-centrations of 0.5–5-fold K_m were employed. For FPP K_m measurements, 0.2–20 μM FPP was used along with 20 μM [^{14}C]IPP. For GGPP K_m measurements, 0.2–20 μM GGPP was used along with 20 μM [^{14}C]IPP. C$_{10}$-GPP at 1–20 μM was also tested as an alternative substrate along with 20–400 μM [^{14}C]IPP for their K_m measurements catalysed by the wild-type UPPS (0.01 μM). All reactions were performed in 100 mM KOH/Hepes buffer, pH 7.5, 50 mM KCl and 0.5 mM MgCl$_2$ at 25 °C in the presence of 0.1 % Triton X-100. To measure the initial rate, 40 μl portions of the reaction mixture were periodically withdrawn within 10 % substrate depletion and mixed with 10 mM EDTA for reaction termination. The radiolabelled products were then ex-tracted with butan-1-ol, and radioactivities associated with either

aqueous or butanol phases were quantified separately by using a Beckman LS6500 scintillation counter to determine the initial reaction velocity. Initial velocity data were fitted to eqn (4) to obtain K_m and k_{cat} values by non-linear regression using the Kaleida-Graph computer program. The k_{cat} was calculated from $V_{max}/[E]$.

$$v_0 = V_{max}[S]/(K_m + [S]) \qquad (4)$$

where v_0 is the initial velocity, [E] the enzyme concentration, [S] the substrate concentration, V_{max} the maximum velocity and K_m the Michaelis constant.

The final products of the UPPS reaction were prepared using 0.1 μM enzyme, 5 μM FPP, GGPP, or GPP and 50 μM [^{14}C]IPP reaction for 6 h. The products were analysed by TLC as described previously [17].

Single-turnover reaction of UPPS using GGPP as a substrate

The single-turnover reaction of UPPS with GGPP was performed by a Kintek RFQ-3 Rapid Chemical Quench apparatus (Kintek Instruments, Austin, TX, U.S.A.) as described previously [15]. The reaction was initiated by mixing 15 μl of the enzyme (10 μM) preincubated with all-*trans*-GGPP (1 μM), and an equal volume of [^{14}C]IPP (50 μM) solution in buffer containing 100 mM Hepes (pH 7.5), 0.5 mM MgCl$_2$ and 50 mM KCl, at 25 °C in the presence of 0.1 % Triton X-100. The enzyme reaction was terminated by quenching with 67 μl of 0.6 M NaOH after specified time periods of 0.2–50 s. The intermediates and products formed during the single-turnover reaction were extracted with butan-1-ol and converted into polyprenols by acid phosphatase and analysed on TLC.

Molecular structural modelling of C$_{55}$-UPP product, C$_{60}$ (eight *cis* double bonds) and assumed C$_{60}$ (nine *cis* double bonds)

The construction of molecular models, structure optimization and conformational analysis were done using the Discover module of Insight II software using the CFF91 forcefield. Computer modelling to predict the three-dimensional structures of C$_{60}$ (eight *cis* double bonds) and C$_{60}$ (nine *cis* double bonds) were performed on a SGI R5000 workstation. By setting the known overall structure of two Triton X-100 molecules in the UPPS active site as in [9], the conformations of the C$_{55}$ and C$_{60}$ products were fully optimized by steepest descent first, and then by conjugate gradient algorithm (see http://www.molvis.indiana.edu/app_guide/InsighII/ for this commonly used modelling method) until root-mean-square derivative < 0.05 kcal · mol^{-1} · Å^{-1} (1 cal = 4.184 J, 1 Å = 0.1 nm), acceptable for molecular modelling.

RESULTS

Role of pyrophosphate of the allylic substrate in binding with UPPS

The diphosphate fluorescent analogue (TFMC-GPP), which was previously abbreviated as CPCF$_3$, serves as an inhibitor ($K_i = 0.57$ μM with respect to FPP) and alternative substrate ($K_m = 0.69$ μM and $k_{cat} = 0.02$ s^{-1}) for *E. coli* UPPS [14]. The fluorescence intensity of this compound quenched by binding with UPPS enzyme can be recovered by adding FPP [14], indicating that the compound binds at the same position as the FPP does. Using stopped-flow technology, the association and dissociation rate constants were found to be $k_{on} = 55.3$ μM^{-1} · s^{-1} and $k_{off} = 31.6$ s^{-1} respectively [14]. The K_d (0.57 μM) value derived from k_{on} and k_{off}, K_i (0.57 μM) and K_m values (0.69 μM) of TFMC-GPP are all similar to the K_m value (0.4 μM) of FPP. In the present study, the same fluorescent FPP analogue TFMC-GP, except with a monophosphate head group, also binds to UPPS
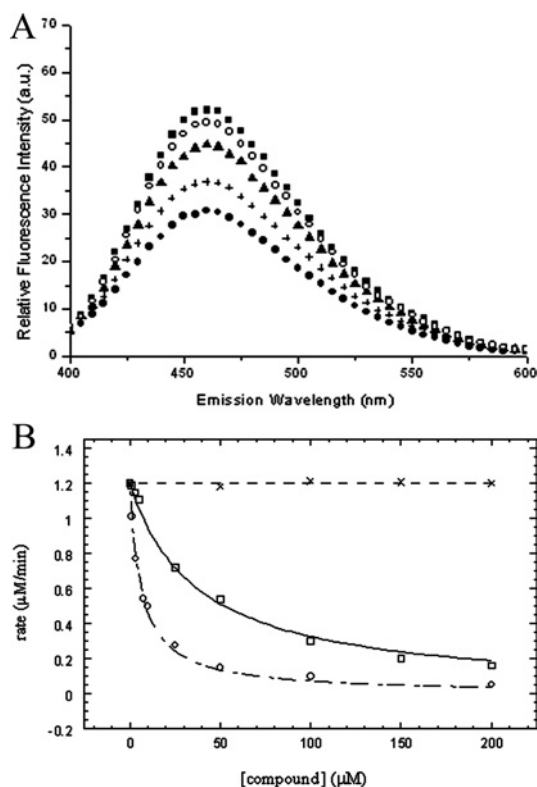

Figure 2   The fluorescent monophosphate analogue of FPP serves as an inhibitor for UPPS

(**A**) The fluorescence of 1 μM TFMC-GP (■) was quenched by adding 1 μM UPPS (●) and gradually recovered by adding 1 (+), 3 (▲) and 5 (○) μM FPP to compete out the inhibitor, indicating that TFMC-GP binds at the same site as FPP does. (**B**) The reaction velocities of UPPS were measured at different concentrations of the TFMC-GP (□), in comparison with TFMC-GPP (○) and farnesol (×). The data for TFMC-GPP were adopted from our previous paper [14]. The K_i values of the compound in the presence of 0.03 μM UPPS, 3 μM FPP and 50 μM IPP were determined to be 5.0 ± 0.3 μM. Farnesol does not inhibit the UPPS reaction at the concentrations indicated.

in a competitive way with respect to FPP. Its fluorescence was reduced by adding UPPS and recovered by displacing with FPP (Figure 2A). However, this monophosphate analogue displays a 9-fold larger inhibition constant ($K_i = 5.0 ± 0.3$ μM) than that of the diphosphate TFMC-GPP (Figure 2B). On the other hand, farnesol, which lacks phosphate, failed to inhibit the UPPS reaction even at 1 mM (Figure 2B shows the data up to 200 μM). Farnesol was not able to displace TFMC-GP from the active site of UPPS in the stopped-flow experiment (results not shown). These results indicate the importance of the diphosphate group for the allylic substrate FPP to bind to the UPPS active site.

The binding of UPPS with the monophosphate analogue was then monitored by using the stopped-flow spectrofluorimeter. A representative stopped-flow trace obtained by mixing 0.5 μM TFMC-GP with an equal volume of 5 μM UPPS is shown in Figure 3(A) ($k_{obs} = 384 ± 21$ s^{-1}). The binding rate constant k_{on} obtained from the slope of the observed rate versus UPPS concentration (the inset in Figure 3A) was $43.5 ± 7$ μM^{-1} · s^{-1}, comparable with the k_{on} (55.3 ± 8 μM^{-1} · s^{-1}) of TFMC-GPP. However, the dissociation constant k_{off} of TFMC-GP (192 ± 14.7 s^{-1}), determined from the stopped-flow competition experiments (Figure 3B) by mixing an equal volume of 0.5 μM enzyme preincubated with 7.5 μM TFMC-GP with 25 μM FPP, was six times faster than that (31.6 s^{-1}) of TFMC-GPP. Thus, the K_d value derived from k_{off}/k_{on} of TFMC-GP is 4.4 μM, approx. 8-fold larger
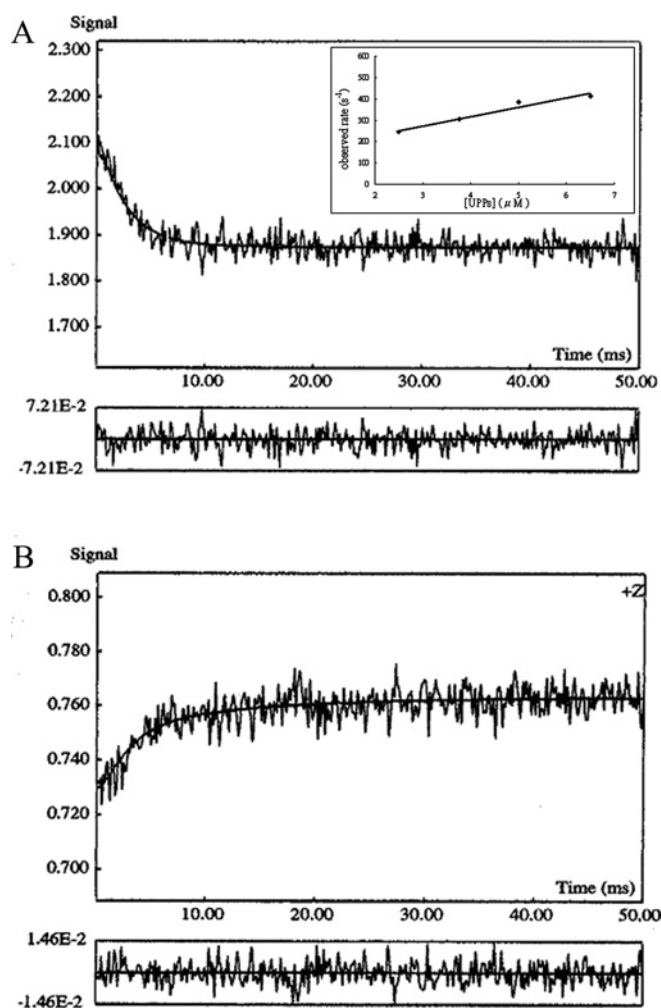
Figure 3   UPPS binding assay by stopped-flow spectrofluorimetry

(**A**) Binding process of UPPS with TFMC-GP was monitored by using the stopped-flow spectrofluorimeter. A representative stopped-trace obtained by mixing 0.5 μM TFMC-GP with an equal volume of 5 μM UPPS is shown. The data were fitted with a single exponential equation to obtain $k_{obs} = 384 \pm 21\ s^{-1}$. The k_{on} was determined from the slope of the plot of k_{obs} values versus concentrations of the compound shown in the inset of this Figure. (**B**) The increase in fluorescence by mixing an equal volume of 0.5 μM enzyme preincubated with 7.5 μM TFMC-GP with 25 μM excessive FPP. By fitting the data with a single exponential equation, the rate constant for the dissociation of the compound from UPPS was determined to be $192 \pm 14.7\ s^{-1}$.

than that of TFMC-GPP. Thus, this difference in K_d value is mainly caused by the larger dissociation rate constant of TFMC-GP.

Role of hydrocarbon moiety of allylic substrate in UPPS reaction

Next, we examined the contribution of the C_{15} hydrocarbon moiety of FPP in binding with UPPS. The C_{10}-GPP was tested as an alternative allylic substrate but showed a 90-fold larger K_m value ($36 \pm 4\ \mu$M) and a 20-fold larger IPP K_m value ($83 \pm 13\ \mu$M) compared with the kinetic parameters of FPP ($K_m = 0.4\ \mu$M) as an allylic substrate and IPP ($K_m = 4\ \mu$M) as a homoallylic substrate. However, the k_{cat} ($1.7 \pm 0.1\ s^{-1}$) of GPP is similar to that ($2.5\ s^{-1}$) for the reaction of FPP and IPP. When the shortest C_5-IPP was used as both allylic and homoallylic substrates, only residual activity was detected ($k_{cat} = 8.5 \times 10^{-5}\ s^{-1}$). On the other hand, the all-*trans* C_{20}-GGPP, a stereoisomer of the C_{20} intermediate of the UPPS reaction, can serve as a satisfactory allylic substrate ($k_{cat} = 2.1\ s^{-1}$, $K_m = 0.3\ \mu$M) with comparable kinetic parameters to those of FPP (Tables 1 and 2).

Table 1   Kinetic parameters of wild-type and mutant *E. coli* UPPS using FPP and IPP as substrates

UPPs	k_{cat} (s^{-1}) (FPP)	K_m (FPP) (μM)	K_m (IPP) (μM)	Rel. k_{cat}*
Wild-type†	2.5 ± 0.1	0.4 ± 0.1	4.1 ± 0.3	1
L85A	0.095 ± 0.01	1.6 ± 0.3	617 ± 123	0.04
L88A	0.23 ± 0.04	2.1 ± 0.7	173 ± 55	0.1
F89A	0.61 ± 0.09	2.6 ± 0.2	84 ± 17	0.24

* k_{cat} relative to that of wild-type.
† Kinetic parameters obtained from [15].

Table 2   Kinetic parameters of wild-type and mutant *E. coli* UPPS using GGPP and IPP as substrates

UPPs	k_{cat} (s^{-1}) (GGPP)	K_m (GGPP) (μM)	K_m (IPP) (μM)	Rel. k_{cat}*
Wild-type†	2.1 ± 0.1	0.3 ± 0.1	13 ± 1	1
L85A	0.18 ± 0.03	1.2 ± 0.3	60 ± 10	0.086
L88A	0.32 ± 0.07	0.7 ± 0.1	42 ± 11	0.15
F89A	0.70 ± 0.11	1.0 ± 0.4	18 ± 2	0.33

* k_{cat} relative to that of wild-type.
† Kinetic parameters obtained from [15].

Since C_5-IPP to C_{20}-GGPP can all act as allylic substrates but with different activities, we also tested whether FPP and GPP can serve as a homoallylic substrate. After incubation for 24 h with a much higher (1 μM) enzyme concentration, still no product was formed from 5 μM [³H]FPP (allylic substrate) and 50 μM FPP (homoallylic substrate) or 5 μM [³H]FPP (allylic substrate) and 50 μM GPP (homoallylic substrate) (results not shown).

L85, L88 and F89 are essential in binding substrate but not important in distinguishing GGPP from FPP

On the basis of our previously solved crystal structure of UPPS in complex with the substrate, interactions between the C_{15} hydrocarbon tail of the FPP molecule and the active site residues of UPPS are mostly hydrophobic [10]. The side-chains of L85, M25, L88, A47, V50, I141, A69, A92 and F89 of UPPS may be involved in the hydrophobic interactions [10]. Three of these residues, L85, L88 and F89, are located on the α3 helix, and move towards the bound FPP during a change in protein conformation [10]. We performed site-directed mutagenesis studies to examine their role in substrate binding and catalysis. As shown in Table 2, the mutants L85A, L88A and F89A showed 4, 5 and 6 times larger FPP K_m values. Apparently, the weaker hydrophobic interaction in the mutant UPPS leads to improper positioning of FPP and also causes a larger IPP K_m and poor activity (IPP is bound after FPP as shown in [8]). The IPP K_m values of the mutants L85A, L88A and F89A are respectively 154, 43 and 21 times larger, and the k_{cat} values of the mutants are 25, 10 and 5 times smaller respectively when compared with the wild-type (Table 1). The L85 side-chain is closer to the electrophilic C_1 of FPP, which is attacked by IPP, thus L85A shows a more remarkably reduced IPP affinity and k_{cat} value.

However, using C_{20}-GGPP as a substrate, the IPP K_m values of three mutant enzymes are larger than that of the wild-type, but significantly smaller than that using FPP as a substrate (Table 2). Furthermore, GGPP K_m values of these mutants are slightly smaller than FPP K_m values. These results suggest that a mutation in which a large amino acid L85, L88 or F89 is replaced with the smaller Ala may give more space in the FPP site to accommodate larger GGPP substrates. However, this effect is not obvious since
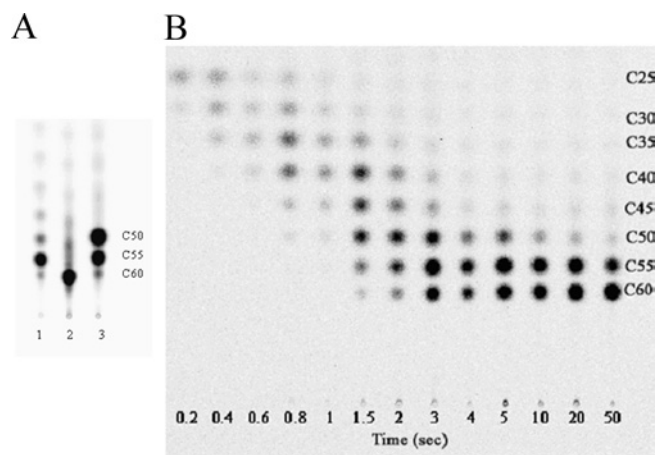
Figure 4   Products generated by the wild-type and the mutant UPPS using FPP, GGPP or GPP as a substrate

The reactions were performed with 1 μM wild-type, 5 μM FPP (lane 1), GGPP (lane 2) or GPP (lane 3), and 50 μM [^{14}C]IPP in a buffer of 100 mM Hepes (pH 7.5), 0.1 mM Mg^{2+}, and 50 mM KCl, in the presence of 0.1 % Triton X-100. (**A**) The major products shown in lanes 1, 2 and 3 are C_{55}, C_{60} and C_{50}, synthesized from FPP, GGPP and GPP respectively. C_{55} was also formed from GPP, but it was still a minor product after an extended reaction time (6 h). (**B**) The formation of intermediates (C_{25}–C_{55}) and product (C_{60}) of UPPS reaction using GGPP as a substrate. The C_{60} formation immediately follows the C_{55} production without delay. This indicates that a UPPS active site can readily accommodate a C_{60} product that contains eight *cis* double bonds.

the wild-type UPPS can still utilize GGPP as a satisfactory substrate as shown above.

Products of C_{20}-GGPP and IPP under steady-state and single-turnover conditions

Interestingly, the enzyme reaction with C_{20}-GGPP and IPP led to a C_{60} final product as judged from TLC (lane 2, Figure 4A), with one extra IPP compared with the C_{55} product synthesized from FPP (lane 1, Figure 4A) under steady-state conditions, where 5 μM GGPP and 50 μM [^{14}C]IPP were used as substrates. Surprisingly, the longer GGPP still underwent eight IPP condensation reactions catalysed by UPPS. To ensure that the formation of C_{60} from GGPP was not due to the extended reaction time, but was immediately formed from C_{55}, a single-turnover reaction where [UPPS] > [GGPP] was performed to monitor the GGPP chain-elongation process in the active site. The reaction was terminated in a series of short periods of time using a rapid-quench apparatus. As shown in Figure 4(B), the intermediates and C_{60} product were formed during the single-turnover of UPPS (10 μM) with GGPP (1 μM), and the C_{60} product was readily formed without any delay from the C_{55}. The radiolabelled [^{14}C]IPP provided the radioactivity of the intermediates and product so that they could be visualized using a phosphoimager by exposing the TLC plate to a film. From the top to the bottom of the TLC, C_{25} to C_{60} products were observed. In contrast, using FPP as the substrate, the C_{20}–C_{55} but not the C_{60} products were formed in the single-turnover reaction catalysed by UPPS [15].

Similar to FPP and GGPP, the shorter GPP also reacted with eight IPPs to form C_{50}, but C_{55} was also formed after an extended reaction time (6 h) (see lane 3, Figure 4A).

Computer prediction of the three-dimensional structures of C_{55}-UPP, C_{60} (eight *cis* double bonds) and assumed C_{60} (nine *cis* double bonds)

We previously proposed that a large residue, L137, serves as a 'floor' at the bottom of the active site tunnel to block further chain
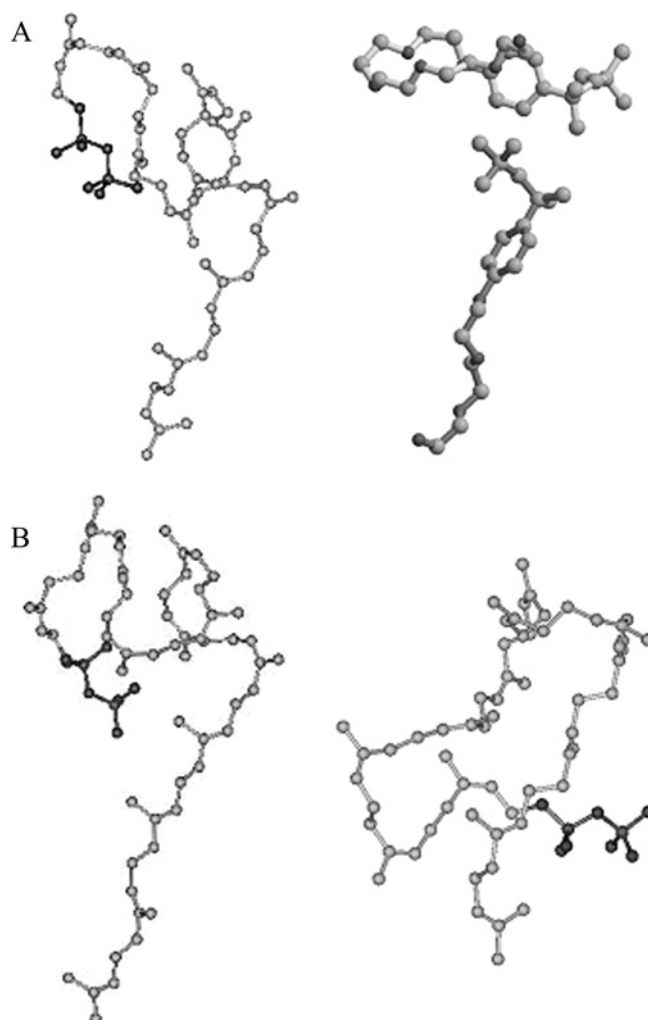

Figure 5   Computer structural modelling of the C_{55} and C_{60} products

(**A**) The molecular shape of C_{55} UPP obtained by energy minimization using the computer program Discover (left panel). This predicted structure of UPP product matches with that of the two Triton X-100 molecules bound in the active site of UPPS (right panel) [9]. (**B**) Molecular shape of C_{60} containing eight *cis* double bonds elongated from all-*trans*-GGPP (left panel) and the assumed C_{60} containing nine *cis* double bonds (right panel). The former adopts a similar shape to that of UPP, whereas the latter has a different shape. The carbon atoms are shown in grey and oxygen atoms in black.

elongation of the C_{55} product so that only a C_{55} product is formed from the reaction of FPP with eight IPPs [12]. The fact that UPPS creates the C_{60} product containing eight *cis* double bonds from GGPP seems to argue against the proposed model. To explain this, we performed computer modelling to derive the most stable structures for both C_{60} products containing eight and nine *cis* double bonds respectively. As shown in Figure 5(A), the energy-minimized structure of C_{55}-UPP (left panel) matches with the overall shape of the two Triton X-100 molecules (right panel) in the active site [9], indicating that the computer-predicted structure of the C_{55} product is truly its structure in the active site. As shown in the left panel of Figure 5(B), the C_{60} product containing eight *cis* double bonds adopts a similar structure to that of the C_{55} product, except with a longer C_5 tail. In contrast, if UPPS catalysed nine IPP condensation reactions using FPP as a substrate, the assumed C_{60} containing nine *cis* double bonds adopts a more enlarged, circular shape (Figure 5B, right panel), which makes the formation of C_{60} (nine *cis* double bonds) unfavourable in the UPPS active site.

From the data presented here, product chain length seems to be determined not only by the L137 at the bottom of the tunnel as shown in Figure 1, but it also seems to be regulated by the space in the upper portion of the active site tunnel, which the *cis* double bonds of the product occupy.

Consistent with this notion, GPP formed C_{50} product to maintain its overall structure of the eight *cis* double bonds. However, the space left between the end of C_{50}-product and L137 is apparently sufficient for C_{50} to twist slightly for condensing with one more IPP to form the C_{55}-product.

DISCUSSION

As demonstrated in the present study, the pyrophosphate head group is important for allylic substrate binding to UPPS. The affinity of the monophosphate FPP analogue was decreased 8-fold mainly due to its faster dissociation rate compared with the diphosphate analogue. Therefore, the loss of the distal phosphate, that forms hydrogen bonds with the side chain and backbone NHs of R30 as well as the side chain NH of R39, accounts for the 8-fold weaker binding. Furthermore, farnesol (an FPP analogue completely lacking the pyrophosphate group) does not interfere with the UPPS reaction, even at the high concentration of 1 mM.

The hydrophobic moiety also contributes significantly to the UPPS–substrate interaction. Whereas UPPS utilizes GGPP with k_{cat} and K_m values similar to that for FPP, the K_m value for GPP as an allylic substrate is remarkably larger. The homoallylic IPP K_m value is also larger when using GPP as an allylic substrate. The larger K_m values of GPP and IPP in this case cannot be due to the competition for the allylic and homoallyic binding sites between GPP and IPP, since GPP could not serve as a homoallylic substrate and IPP serves as a poor allylic substrate with extremely low activity, as shown by the data presented here. This indicates that the allylic substrate that is 5 or 10 carbons shorter than FPP causes remarkably lower affinity and reactivity, but if it is 5 carbons larger (GGPP) it serves as an equally good allylic substrate.

However, using all-*trans* C_{20}-GGPP as an alternative substrate results in the production of the longer C_{60} compared with the normal product C_{55}. *In vivo*, GGPP could lead to C_{60} product, which may not be as satisfactory a lipid carrier as UPP. This may become an important issue since more and more attempts have been made to produce useful isoprenoids using *E. coli* as a factory by overproducing GGPP, which serves as a precursor for many isoprenoid compounds [18–20]. Indeed, it has been observed that high-level expression of the plasmid-encoded *crtE* gene (a GGPP synthase) causes cytotoxicity of the *E. coli* host cells [21]. We also observed the same effect when *E. coli* expressed GGPP synthase (results not shown). This could be due to the incorporation of the C_{60} polyprenol, which is not an efficient lipid carrier, and/or IPP pools being depleted due to other primary metabolic biosyntheses. When other genes are introduced into the engineered *E. coli*, which can transform GGPP into the desired products, *E. coli* should still grow well.

The hydrophobic residues, including L85, L88 and F89, interact with the hydrocarbon moiety of FPP in the UPPS active site. These residues ensure the correct position and orientation of the allylic substrate FPP for an efficient nucleophilic attack by IPP. The substitution of L85, L88 and F89 with Ala lowered the substrate affinity and k_{cat} values (Tables 1 and 2). It is notable that these three amino acids located on the α3 helix interact with the substrate only when FPP is bound and the closed conformation is formed [10,22]. It has been shown that the flexible loop (amino acids 72–83) preceding the α3 helix may pull this helix closer to the bound FPP substrate in the closed conformation [22]. As shown

in the present study, amino acids such as L85, L88 and F89 on the α3 helix directly participate in substrate binding and catalysis.

On the basis of our results, the product chain length determination of UPPS may not only be dependent on the bottom part of the active site tunnel as shown in Figure 1(A), but may also be regulated by the space in the upper portion of the active site tunnel of UPPS. In general, *cis*-type linear prenyltransferases synthesize much longer chain-length products than *trans*-type enzymes. Rubber prenyltransferase (*cis*-type) can catalyse the incorporation of thousands of IPP units into FPP initiator [23], but *trans*-type enzymes identified thus far only generate up to a C_{50} product [24]. From the three-dimensional structures of *cis*-type UPPS and *trans*-type OPPS that we solved, we found that the UPPS is broader at the top portion of the tunnel (funnel-like) compared with the *trans*-type (cylinder-like) OPPS, which makes the all-*trans* C_{40} product to have a linear shape. The molecular shapes of the active sites of these *cis*- and *trans*-type prenyltarnsferases are apparently important for controlling the chain lengths of the products. For the *cis*-type rubber prenyltransferases, which form extremely large polymers [25], we predict that they must have a spacious top portion of the tunnel-like active site crevice plus a bottom and/or side opening to allow the continuation of chain elongation. This is supported by our computer-generated structural model for the rubber prenyltransferase (results not shown), but yet to be verified by the crystal structure.

REFERENCES

1 Liang, P. H., Ko, T. P. and Wang, A. H.-J. (2002) Structure, mechanism and function of prenyltransferases. Eur. J. Biochem. **269**, 3339–3354
2 Ogura, K., Koyama, T. and Sagami, H. (1997) Polyprenyl diphosphate synthases. Subcellular Biochem. **28**, 57–87
3 Poulter, C. D. and Rilling, H. C. (1982) Prenyl transferases and isomerase. In Biosynthesis of Isoprenoid Compounds, vol. 1 (Porter, J. W. and Spurgeon, S. L., eds.), Chapter 4, pp. 161–224, John Wiley & Sons, New York
4 Ogura, K. and Koyama, T. (1998) Enzymatic aspects of isoprenoid chain elongation. Chem. Rev. **98**, 1263–1276
5 Chen, A., Kroon, P. A. and Poulter, C. D. (1994) Isoprenyl diphosphate synthases: protein sequence comparisons, a phylogenetic tree, and predictions of secondary structure. Protein Sci. **3**, 600–607
6 Tarshis, L. C., Proteau, P. J., Kellogg, B. A., Sacchettini, J. C. and Poulter, C. D. (1996) Regulation of product chain length by isoprenyl diphosphate synthases. Proc. Natl. Acad. Sci. U.S.A. **93**, 15018–15023
7 Guo, R. T., Kuo, C. J., Chou, C. C., Ko, T. P., Shr, H. L., Liang, P. H. and Wang, A. H.-J. (2004) Crystal structure of octaprenyl pyrophosphate synthase from hyperthermophilic *Thermotoga maritima* and mechanism of product chain length determination. J. Biol. Chem. **279**, 4903–4912
8 Chen, Y. H., Chen, A. P.-C., Chen, C.-T., Wang, A. H.-J. and Liang, P. H. (2002) Probing the conformational change of *Escherichia coli* undecaprenyl pyrophosphate synthase during catalysis using an inhibitor and tryptophan mutants. J. Biol. Chem. **277**, 7369–7376
9 Chang, S. Y., Ko, T. P., Liang, P. H. and Wang, A. H.-J. (2003) Catalytic mechanism revealed by the crystal structure of undecaprenyl pyrophosphate synthase in complex with sulfate, magnesium, and Triton. J. Biol. Chem. **278**, 29298–29307
10 Chang, S. Y., Ko, T. P., Chen, A. P.-C., Wang, A. H.-J. and Liang, P. H. (2004) Substrate binding mode and reaction mechanism of undecaprenyl pyrophosphate synthase deduced from crystallographic studies. Protein Sci. **13**, 971–978
11 Varki, A., Cummings, R., Esko, J., Freeze, H., Hart, G. and Marth, J. (1999) Bacterial polysaccharides. In Essentials of Glycobiology, Chapter 21, pp. 322–325, Cold Spring Harbor Laboratory Press, Plainview, NY
12 Ko, T. P., Chen, Y. K., Robinson, H., Tsai, P. C., Gao, Y.-G., Chen, A. P.-C., Wang, A. H.-J. and Liang, P. H. (2001) Mechanism of product chain length determination and the role of a flexible loop in *Escherichia coli* undecaprenyl-pyrophosphate synthase catalysis. J. Biol. Chem. **276**, 47474–47482
13 Apfel, C. M., Takacs, B., Fountoulakis, M., Stieger, M. and Keck, W. (1999) Use of genomics to identify bacterial undecaprenyl pyrophosphate synthetase: cloning, expression, and characterization of the essential uppS gene. J. Bacteriol. **181**, 483–492

14 Chen, A. P.-C., Chen, Y. H., Liu, H. P., Li, Y. C., Chen, C.-T. and Liang, P. H. (2002) Synthesis and application of a fluorescent substrate analogue to study ligand interactions for undecaprenyl pyrophosphate synthase. J. Am. Chem. Soc. **124**, 15217–15224

15 Pan, J. J., Chiou, S. T. and Liang, P. H. (2000) Product distribution and pre-steady-state kinetic analysis of *Escherichia coli* undecaprenyl pyrophosphate synthase reaction. Biochemistry **39**, 10936–10942

16 Segel, I. H. (1993) Enzyme Kinetics: Behavior and Analysis of Rapid Equilibrium and Steady-state Enzyme Systems. In Wiley Classics Library edn, pp. 100–108, John Wiley and Sons, New York

17 Pan, J. J., Yang, L. W. and Liang, P. H. (2000) Effect of site-directed mutagenesis of the conserved aspartate and glutamate on *E. coli* undecaprenyl pyrophosphate synthase catalysis. Biochemistry **39**, 13856–13861

18 Wang, C. W., Oh, M. K. and Liao, J. C. (1999) Engineered isoprenoid pathway enhances astaxanthin production in *Escherichia coli*. Biotechnol. Bioeng. **62**, 235–241

19 Huang, Q., Roessner, C. A., Croteau, R. and Scott, A. I. (2001) Engineering Escherichia coli for the synthesis of taxadiene, a key intermediate in the biosynthesis of taxol. Bioorg. Med. Chem. **9**, 2237–2242

20 Ravanello, M. P., Ke, D., Alvarez, J., Huang, B. and Shewmaker, C. K. (2003) Coordinate expression of multiple bacterial carotenoid genes in canola leading to altered carotenoid production. Metab. Eng. **5**, 255–263

21 Math, S. K., Hearst, J. E. and Poulter, C. D. (1992) The crtE gene in *Erwinia herbicola* encodes geranylgeranyl diphosphate synthase. Proc. Natl. Acad. Sci. U.S.A. **89**, 6761–6764

22 Chang, S. Y., Chen, Y. K., Wang, A. H.-J. and Liang, P. H. (2003) Identification of the active conformation and the importance of length of the flexible loop 72-83 in regulating the conformational change of undecaprenyl pyrophosphate synthase. Biochemistry **42**, 14452–14459

23 Cornish, K. (2001) Similarities and differences in rubber biochemistry among plant species. Phytochemistry **57**, 1123–1134

24 Koyama, T. (1999) Molecular analysis of prenyl chain elongating enzymes. Biosci. Biotechnol. Biochem. **63**, 1671–1676

25 Asawatreratanakul, K., Zhang, Y. W., Wititsuwannakul, D., Wititsuwannakul, R., Takahashi, S., Rattanapittayaporn, A. and Koyama, T. (2003) Molecular cloning, expression and characterization of cDNA encoding cis-prenyltransferases from Hevea brasiliensis. A key factor participating in natural rubber biosynthesis. Eur. J. Biochem. **270**, 4671–4680